

Influence of Fermions on Vortices in SU(2)-QCD

Zeinab Dehghan, Sedigheh Deldar

Department of Physics, University of Tehran, Iran

Manfried Faber, Rudolf Golubich

Atominstitut, Techn. Univ. Wien, Operngasse 9, A-1040 Wien

faber@kph.tuwien.ac.at

Roman Höllwieser

Department of Physics, Bergische Universität Wuppertal, Germany

April 6, 2021

Abstract

Gauge fields control the dynamics of fermions, also a back reaction of fermions on the gauge field is expected. This back reaction is investigated within the vortex picture of the QCD vacuum. We show that the center vortex model reproduces the string tension of the full theory also with the presence of fermionic fields.

1 Introduction

The QCD vacuum is highly nontrivial and has magnetic properties, as we know since Savvidy's article [1]. The QCD vacuum should explain the non-perturbative properties of QCD, among them confinement [2] and chiral symmetry breaking [3]. Lattice QCD puts the means at our disposal to answer the question about the important degrees of freedom of this non-perturbative vacuum. In the center vortex picture [4, 5, 6] the QCD vacuum is seen as a condensate of closed quantized magnetic flux tubes. These flux tubes have random shapes and evolve in time and therefore form closed surfaces in the dual space. They may expand and shrink, fuse and split and percolate in the confinement phase in all space-time directions and pierce Wilson loops randomly. Thus, Wilson loops follow asymptotically an exponential decay with the area. This is the area law of Wilson loops, which allows to attribute the string tension to center vortices. The finite temperature phase transition is characterized by a loss of center symmetry and correspondingly by a loss of percolation in time direction, where vortices get static and spatial Wilson loops keep showing the area law behaviour.

Color electric charges are sources of electric flux according to Gauss's law. The electric flux between opposite colour charges does not like to penetrate this magnetic "medium" and shrinks to the well-known electric flux tube. On the other hand, the magnetic flux does not like to enter the electric string. Since fermions carry color charges, their dynamics is controlled by the gauge field. The presence of a fermion condensate is expected to suppress the quantized magnetic flux lines, and as a result the gluon condensate and therefore the string tension are reduced. Since, as usual, the lattice spacing is determined via the string tension, taking into account dynamical fermions leads to a decrease of the lattice spacing. In this article we show a careful investigation of the string tension within the vortex picture of the QCD vacuum.

SU(2) and SU(3) QCD have equivalent non-perturbative properties. In a first study, we restrict our analysis to the simpler case of SU(2)-QCD. The most important difference between SU(2) and SU(3) QCD is the order of the finite temperature phase transition for a pure gluonic Lagrangian. There is a natural explanation of this differences from the structure of SU(2) and SU(3) vortices. There is only one non-trivial center element in the group SU(2) and therefore one type of center vortices, whereas there are two non-trivial center elements for SU(3) and two types of vortices, allowing two vortices of the same type to

fuse to the other type. This leads to more stable structure of the net of vortices for SU(3) and to a first order phase transition, whereas in SU(2) the transition is of second order.

We investigate the fermionic backreaction on the gluonic degrees of freedom in SU(2) QCD. Visualizing the distribution of the center vortex, this backreaction can be easily observed, see Figure 1. It is difficult to draw a closed surface in four dimensions. Therefore we restrict ourselves to the three dimensional diagram of a time-slice and indicate the continuation to other slices by line stubs. One can clearly see that dynamical fermions decrease the percolation of vortices. We want to quantify the effect in more detail. We

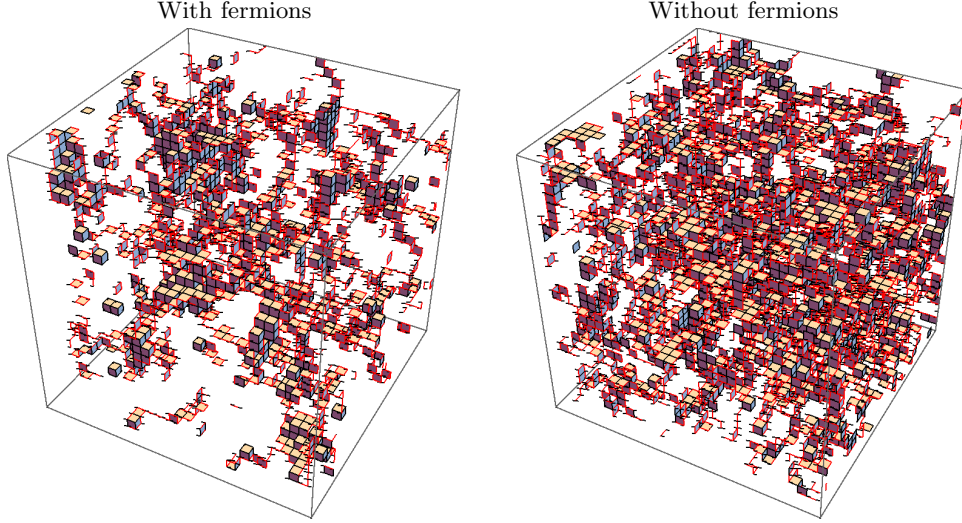


Figure 1: The closed vortex surface is visualized by showing the dual P-plaquettes of 3 dimensional lattice slices. Stubs of red lines indicate plaquettes that are not fully part of the lattice slice shown. We clearly see that with fermions (left) an overall smaller amount of P-plaquettes is observed compared with the pure gluonic case (right). In both cases one big cluster dominates.

are especially interested in the *center vortex model* [4, 5, 6] and its sensitivity to the fermionic backreaction. This work compares four different estimates of the string tension, with and without fermions, in the full theory and in the vortex picture.

- via the potential without fermionic fields calculated only using the center degrees of freedom,
- via the potential with fermionic fields calculated only using the center degrees of freedom,
- via the potential without fermionic fields calculated using the full theory,
- via the potential with fermionic fields calculated using the full theory.

With this comparison, we study the sensitivity of the center vortex model to the fermionic backreaction. Of further interest is the influence of fermionic fields on the geometric structure of the center vortex surface.

Our work is based on the QCD path integral which defines the vacuum to vacuum transition amplitude. In lattice QCD we usually evaluate this amplitude on a lattice periodic in euclidean time. Inserting a complete set of eigenstates of QCD with the quantum numbers of the vacuum in this amplitude results in an exponential decay of the eigenstates with the physical time extent aN_t of the lattice, where a is the lattice spacing and N_t the number of lattice sites in time direction. The inverse of this time extent acts therefore as a temperature of the ensemble. In a Monte-Carlo simulation, the states are occupied with the corresponding Boltzmann factor. The higher the excitation, the smaller is the Boltzmann factor and the more difficult is the measurement of its properties. Finally, the excited states are vanishing in the noise. The potential, as well as the string tension, can be calculated using *Wilson loops* $W(R, T)$, which are observables with the quantum numbers of the vacuum

$$W(R, T) = \text{Tr} \mathcal{P} e^{i g \int_{R \times T} A_\mu^a(x) t_a dx^\mu}. \quad (1)$$

A loop of size $R \times T$ in space-time represents the world-line of a quark-antiquark system at distance R immersed in the QCD vacuum for time T . On an euclidean lattice in SU(2)-QCD, the path ordered loop is determined by the product of link variables $U_\mu(x) \in \text{SU}(2)$ along the loop. Inserting a complete set of eigenstates of the quark-antiquark system into the expectation value $\langle W(R, T) \rangle$, the contributions of the eigenstates decay exponentially in euclidean time T . The expectation values of Wilson loops can therefore be expanded in a series of eigenstates of the quark-antiquark system

$$\langle W(R, T) \rangle = \sum_{i=0}^{\infty} c_i e^{-\varepsilon_i(R)T}, \quad (2)$$

For large times, $\langle W(R, T) \rangle$ is dominated by the ground state energy $\varepsilon_0(R)$. The more precise we determine $\lim_{T \rightarrow \infty} \langle W(R, T) \rangle$, the better is the precision of the quark-antiquark potential $V(R) := \varepsilon_0(R)$. Since the energy of the quark-antiquark system increases with the distance R , it follows from the above discussion that for increasing R the signal for $V(R)$ is vanishing soon in the noise. How we handle this noise and how center vortices are detected, is described in section 2. We assume, that the potential is dominated by a Coulombic part at small R but rises linearly for large R ,

$$\varepsilon_0(R) = V(R) = V_0 + \sigma R - \frac{\alpha}{R}. \quad (3)$$

We use $\langle W(R, T) \rangle$ to approximate $\varepsilon_0(R)$, denoted as *1-exp fit*. V_0 parametrizes the scale dependent self-energy of the quark-antiquark sources. The center degrees of freedom are expected to have vanishing contributions from the short range fluctuations, hence we describe the potential within these degrees of freedom by

$$V_{\text{CP}}(R) = v_0 + \sigma_{\text{CP}} R. \quad (4)$$

The aim of this article is to investigate whether we can understand the string tension and its modification in the presence of fermions in the vortex model of confinement. Further, we present and discuss conceptual improvements to gauge fixing procedure, required for the center vortex detection.

2 Materials and Methods

This section starts with a description of the parameters of the lattice configurations, used for our analysis. Then, our method of detecting center vortices with some novel improvements is discussed. We explain, how the information about the geometric structure of the vortex surface can be acquired by smoothing procedures and then we end with a detailed explanation of our method to extract the potential from Wilson loops. In each subsection we list the intermediary results.

2.1 Simulation specifications

We study the configurations described in Ref. [7] for chemical potential $\mu = 0$ with S_G defined by a tree level improved Symanzik gauge action [8, 9].

$$S_G = \beta \left(c_0 \sum_{\square} \left(1 - \frac{1}{2} \text{Tr } \square \right) + c_1 \sum_{\square\square} \left(1 - \frac{1}{2} \text{Tr } \square\square \right) \right) \quad (5)$$

with coefficients $c_0 = 5/3$ and $c_1 = -1/12$. The first sum corresponds to the Wilson action with \square indicating single unoriented plaquettes, the second sum uses rectangular Wilson loops build by 6 links, symbolized by $\square\square$. The inverse coupling is defined as $\beta = \frac{4}{g^2}$ for SU(2).

For the fermionic degrees of freedom staggered fermions are used with an action of the form

$$S_F = \sum_{x,y} \bar{\psi}_x M(m)_{x,y} \psi_y + \frac{\lambda}{2} \sum_x (\psi_x^T \tau_2 \psi_x + \bar{\psi}_x \tau_2 \bar{\psi}_x^T) \quad (6)$$

with τ_i being the Pauli matrices and

$$M(m)_{xy} = ma\delta_{xy} + \frac{1}{2} \sum_{\nu=1}^4 \eta_{\nu}(x) \left[U_{x,\nu} \delta_{x+h_{\nu},y} - U_{x-h_{\nu},\nu}^{\dagger} \delta_{x-h_{\nu},y} \right], \quad (7)$$

where $\bar{\psi}, \psi$ are staggered fermion fields, a is the lattice spacing, m is the bare quark mass, $U_{x,\nu}$ a SU(2) element corresponding to a link at position x in direction μ and $\eta_{\nu}(x)$ are the standard staggered phase factors: $\eta_1(x) = 1, \eta_{\nu}(x) = (-1)^{x_1+\dots+x_{\nu-1}}, \nu = 2, 3, 4$. The total action is given by $S = S_G + S_F$. Integrating out the fermionic degrees of freedom, the partition function with $N_f = 2$ is given by

$$Z = \int DU e^{-S_G} (\det(M^{\dagger}M) + \lambda^2)^{\frac{1}{4}}. \quad (8)$$

The properties of 1000 configurations of size 32^4 with $m_{\pi} = 740(40)MeV$, $\lambda = 0.00075$ and $\beta = 1.8$ are compared to 1000 pure gluonic configurations at the same inverse coupling β . The results of the evaluations for center projected configurations are much more stable and need much more computational resources. Therefore, we restrict the computations to 40 configurations with maximal distance. For each of these 40 configurations we center project 100 random gauge copies. With this new method we try to overcome the Gribov ambiguity problem, which *Direct Maximal Center Gauge* (DMCG) usually suffers from.

For both sets of 1000 configurations we extract the potentials from all available Wilson loop data and compare them with the string tensions resulting from the two sets of 40×100 center projected configurations. In this way we try to answer the question, if in the presence of dynamical fermions the center degrees of freedom determine the string tension of the gluonic flux tube in quark-antiquark systems.

2.2 Center vortex detection

Assuming that center excitations are the relevant degrees of freedom for confinement, we detect these center vortices within the lattice configurations. We first identify gauge matrices $\Omega(x) \in \text{SU}(2)$ at each site x^{μ} maximizing the functional

$$R_F = \sum_x \sum_{\mu} | \text{Tr}[\dot{U}_{\mu}(x)] |^2 \quad \text{with} \quad \dot{U}_{\mu}(x) = \Omega(x + e_{\mu}) U_{\mu}(x) \Omega^{\dagger}(x). \quad (9)$$

After fixing the gauge, the link variables $\dot{U}_{\mu}(x)$ are projected on the center degrees of freedom, that is ± 1 for SU(2), to neglect short range properties and keep only long range effects

$$U_{\mu}(x) \rightarrow Z_{\mu}(x) \equiv \text{signTr}[U_{\mu}(x)]. \quad (10)$$

After performing the center projection, the center projected plaquettes resulting from the vortex detection are the products of four center elements. The projected plaquettes are non-trivial, known as P-plaquettes, $U_{\square} = -1$, if one or three links are non-trivial. In the four dimensional lattice a given link belongs to 6 plaquettes. On the dual lattice the corresponding 6 plaquettes build the surface of a cube. Therefore, the duals of P-plaquettes form closed surfaces, dual P-vortices which correspond to the closed flux line evolving in time.

This procedure is the original DMCG [10] in which a gradient climb with *over relaxation* was used to maximize the gauge functional. From a few gauge copies only, produced in this way, the one with the highest value of the functional is usually chosen for further analysis. This method leads to promising results, but improvements at maximizing the gauge functional using *simulated annealing* have brought a flaw to light - the many local maxima of R_F not necessarily correspond to the same physics: Bornyakov et al. [11] have shown that there exist local maxima of the gauge functional that underestimate the string tension. We have been able to resolve these problems for smaller lattices using improved version of the gauge fixing routines based on non-trivial center regions [12, 13, 14], but our implementation was not capable to handle the big lattices used in this work. Taking a closer look at the problem at hand, we can look for a different approach. We now consider Creutz ratios to estimate the string tension

$$\sigma \approx \chi(R) = -\ln \frac{\langle W(R+1, R+1) \rangle \langle W(R, R) \rangle}{\langle W(R, R+1) \rangle \langle W(R+1, R) \rangle}, \quad (11)$$

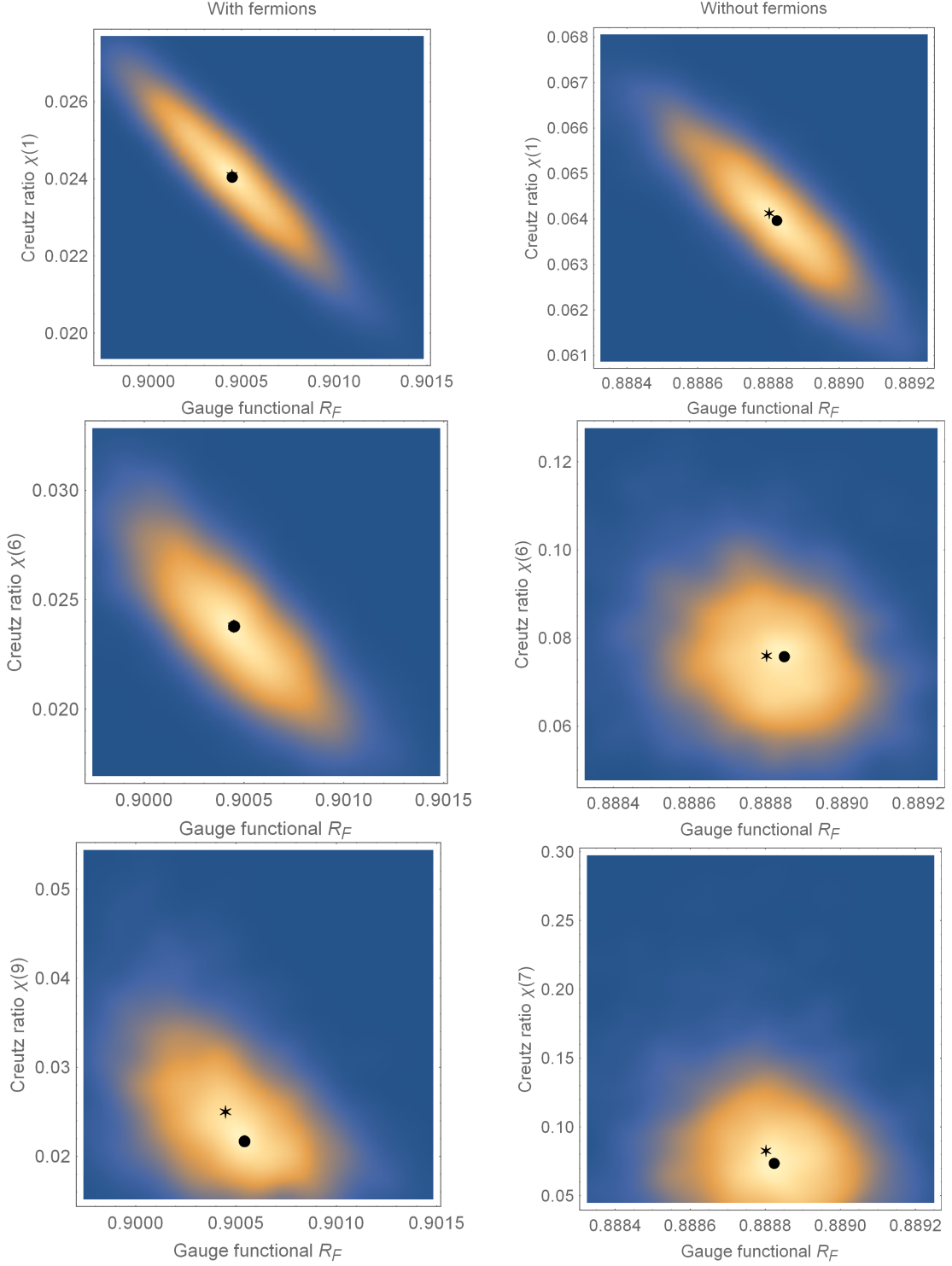


Figure 2: These probability densities specify the relation between the values of gauge functional and Creutz ratio for individual configurations. This determination is based on 40 configurations with 100 gauge copies for the configurations with dynamical fermions (left) and without (right). For Creutz ratios of small Wilson loops we observe a nearly linear relation. With increasing size of the Wilson loops this correlation weakens. We marked the average values (star) and the most probable values (circle) of the distributions.

with Wilson loops $W(R, R)$ of size $R = T$. Some probability densities for the relation between the values of the gauge functional R_F and the Creutz ratio $\chi(R)$ for individual configurations are shown in Fig. 2. This determination is based on 40 configurations with 100 gauge copies for configurations with dynamical fermions (left) and without (right). For Creutz ratios of small Wilson loops we observe a nearly linear relation between the two quantities reflecting the finding of Ref. [11]: There exist gauge copies of the configurations with maximal R_F and very low σ . With increasing size of Wilson loops this correlation weakens. Nevertheless, the request to maximize the gauge functional (9) fails.

Another observation is of high interest: extremely small and large values of the gauge functional are strongly suppressed in the probability densities. Instead of looking for higher local maxima of the gauge functional, we propose a different approach: “ensemble averaged maximal center gauge” (EaMCG). We produce many random gauge copies, approach the next local maximum by the gradient method and take the average of the ensemble. The idea is that not the best local maximum alone carries the physical meaning, but the average over all local maxima do: Maxima with a higher value of the gauge functional result in a reduced string tension, but they are not dominating the ensemble. The same holds for lower valued maxima, possibly overestimating the string tension.

Taking again a look at Fig. 2, it can be seen that the average values and the most probable values are in good agreement for small loops. This is shown in more detail in Fig. 3 for Creutz ratios of different loop-sizes. The differences increasing with loop sizes can probably be explained by the lack of statistics for the Creutz ratios of single configurations. Until the values start to deviate from one another, there is a variation of 10% over the whole R -region. Despite the low statistics of a single configuration, the intermediate loop sizes already reproduce the asymptotic behaviour and let us expect the possibility for a more precise determination. First averaging over Wilson loops and then calculating Creutz ratios gives much more stable results, see $\chi_W(R)$ in Fig. 3. The final estimate of the string tensions in Sects. 2.4 and 3 will be based on the determination of the potential.

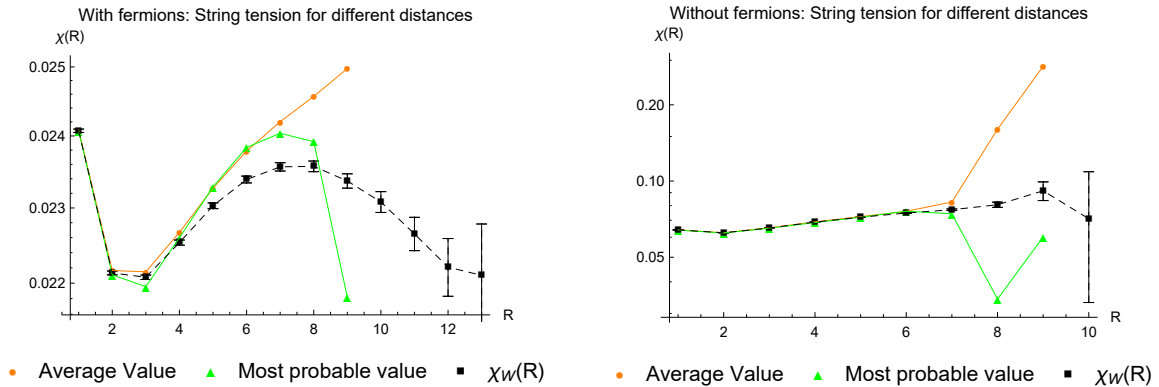


Figure 3: The Average and the most probable value of $\chi(R)$ are compared for simulations with and without fermions. This complements the probability densities of Fig. 2. The increasing discrepancy between the two quantities with raising R can probably be explained by the low precision of Creutz ratios of single configurations. Until the values start to deviate from one another, the variations of $\chi(R)$ are of the order of 10%. For comparison we show also the more precise Creutz ratios $\chi_W(R)$ extracted from averages of Wilson loops.

So far, we have calculated the Creutz ratios for single configurations of the ensemble and have taken the average afterwards. The EaMCG itself does not average over Creutz ratios, but combines first the Wilson loops of all gauge copies and configurations. From this fact it is possible to extract the quark anti-quark potential, which allows a more precise determination of the string tension from the center vortex model.

In the respective single configurations we observe one percolating large cluster that is surrounded and traversed by small fluctuations. These result in an increased number of P-plaquettes that do not contribute to the string tension. Analysing these distortions we gain insight on the influence of fermions on the geometric structure of the vortex surface.

2.3 Smoothing the vortex surface

There exist several procedures for smoothing the vortex surface by removing distortions. These procedures are discussed in detail in Ref. [15]. They do not modify the long range effects of the configuration. To get information about the smoothness of the vortex surface with and without fermions we use the smoothing steps depicted in Fig. 4. Not depicted is *smoothing 0*, which removes unit-cubes. The procedure cuts out

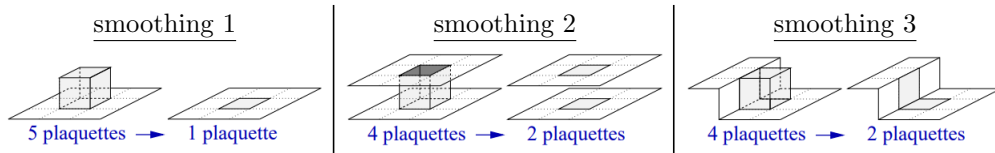


Figure 4: The effect of the smoothing procedures on the vortex surface is depicted, taken from [16, Fig.5.8.]. We distinguish *warts* (left), *bottlenecks* (middle) and *stumbling blocks* (right). Not depicted are *unit cubes*.

parts of the vortex surface and closes the emerging holes with a flat surface. In this way, short range fluctuations of the vortex surface get flattened. We first count the P-plaquettes without any smoothing performed, then the loss of P-plaquettes for the respective smoothing procedure is determined. The results are given in Table 1. This quantifies the percentage of the respective structures depicted in Fig. 4. When

P-plaquette reduction	smoothing 0	smoothing 1	smoothing 2	smoothing 3
With fermions	12.5%	10.1%	24%	10.2%
Without fermions	7%	10.6%	27.8%	10.9%

Table 1: Reduction of the total count of P-plaquettes for different smoothing procedures.

fermions are present, we have clearly a higher proportion of unit cubes and a lower proportion of bottlenecks than without fermions.

By restricting this analysis to the single percolating vortex cluster, we gain information about the long range excitations. The results are given in Table 2. The reduction in the proportion of bottlenecks is also

reduction within cluster	smoothing 1	smoothing 2	smoothing 3
With fermions	8.6%	24.5%	8.8%
Without fermions	9.6%	28.1%	10%

Table 2: Reduction of P-plaquettes for the percolating vortex cluster for different smoothing procedures.

seen here. The presence of fermions leads to a smoother surface of the percolating cluster.

2.4 Potential fits and noise handling

When extracting the potential from Wilson loops, two effects have to be taken care of:

- for small areas the loop averages are influenced by short range fluctuations,
- with increasing area the data suffers from statistical noise and soon the errors get larger than the signal.

An example for an 1-exponential fit to Wilson loops $\langle W(R, T) \rangle$ for given R and $T \geq T_i$, see Eq. (2), is shown in the left diagram of Fig. 5. The dependence of this example on the initial $T = T_i$ is depicted in the right diagram. At lower T_i , an increase of T_i causes large changes of the fit parameters, but with growing T_i these changes become smaller until a most stationary point is reached which may be hidden behind a strong increase of errorbars. With the naked eye one greps data that result in quite good fits, but finding analytic or numeric criteria for the choice of T_i proofs difficult. The smallest change of the values of the fit parameters, the smallest errorbars of Wilson loops and a rapid increase of the p-value of

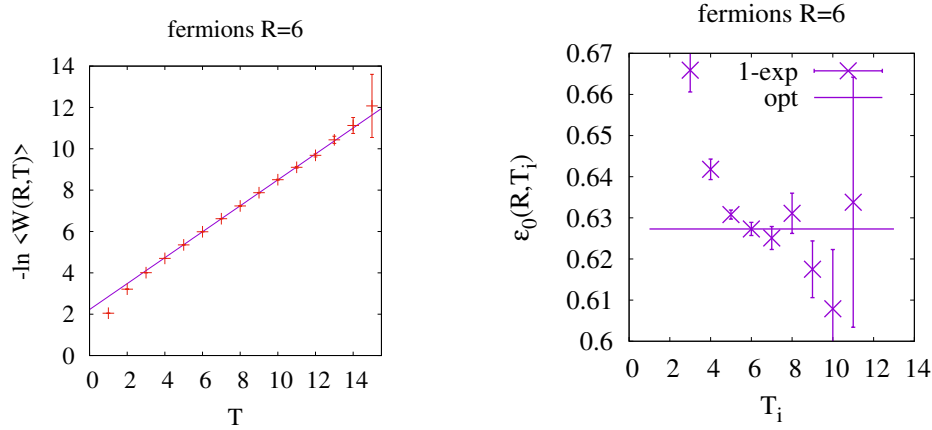


Figure 5: Left: Example of the optimal 1-exponential fit of Wilson loops for given R . Right: Dependence of $\varepsilon_0(R, T_i)$ on the fit region $T \geq T_i$. The line marks the fit for the optimal value for T_i .

the fits often coincide, but this is not a general rule. Our criteria to choose T_i is based on identifying the first local minimum of an error quantifier

$$\text{Err} := \frac{2}{3} \langle \Delta_{\delta i} \rangle + \frac{1}{3} \langle \Delta_{\text{err}} \rangle. \quad (12)$$

Here, $\langle \Delta_{\delta i} \rangle$ denotes the average change of the fit parameter $\varepsilon(R, T_{i \pm 1})$ when decreasing or increasing T_i ; and $\langle \Delta_{\text{err}} \rangle$ denotes the average over the error bars of $\varepsilon(R, T_{i-1})$, $\varepsilon(R, T_i)$ and $\varepsilon(R, T_{i+1})$. The weight factors are chosen to avoid the choice of occasionally nearly stationary regions with large errorbars. For $R > 3$ we prevent any further increase of T_i , because with increasing R the error bars start to grow earlier. The example in Figure 5 tries to convince that the selection of T_i based on the error quantifier results in an optimal fits under the boundary conditions of systematic deviations for low T_i and increasing error bars for high T_i . Using this procedure we determine the potential for the whole range of R -values, which allows to extract the slope of the potential at large values of R .

3 Summarized Results and Discussion

The fermionic backreaction on the string tension is clearly observed in the full theory as well as for EaMCG, where the link variables of the gauge field are projected to Z_2 . The potentials for the gluonic and fermionic configuration are depicted in Fig. 6 and compare the full $SU(2)$ theory with the Z_2 theory. The string tension was extracted by fitting the respective Eq. (3) or (4) to the data describing the potential. The resulting parameters of these fits are given in Table 3. The relevant parameters to compare are σ and σ_{CP} . Without fermions both estimates for σ are compatible within errors to one another: In the full $SU(2)$

theory parameter	SU(2)			Z ₂	
	V ₀	σ	α	v ₀	σ _{CP}
gluonic	0.5175(38)	0.0756(12)	0.2326(26)	-0.0366(8)	0.07691(13)
fermionic	0.5464(27)	0.0199(9)	0.2414(19)	0.01027(13)	0.02291(5)

Table 3: The parameters for the fits according Eq. (4) and Eq. (3) in Fig. 6 allow a direct comparison of the respective string tensions. A strong suppression of the Coulomb part can be seen in the Z_2 theory.

we observe $\sigma = 0.0756(12)$ compared to $\sigma_{\text{CP}} = 0.07691(13)$ in the Z_2 description. With fermions the full $SU(2)$ theory results with $\sigma = 0.0199(9)$ a lower value than the Z_2 theory with $\sigma_{\text{CP}} = 0.02291(5)$. In

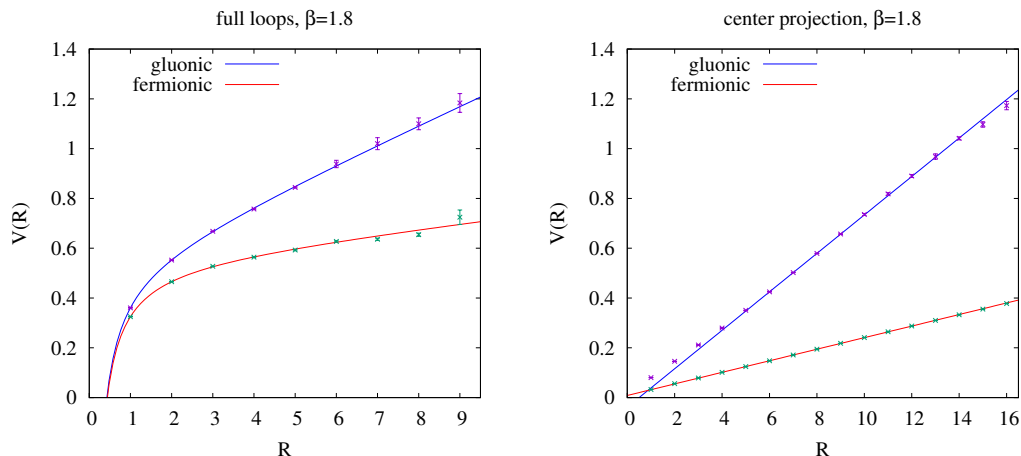


Figure 6: Left: Potential $V(R)$ in lattice units between two sources in the fundamental representation. There is a large difference between the string tensions for pure gluonic configurations (“gluonic”) and in the presence of one species of dynamical fermions. Right: Potential extracted from Wilson loops after ensemble averaged maximal center projection are depicted for pure gluonic configurations and for configurations with dynamical fermions. Due to the removal of short range fluctuations the potentials are in both cases almost linearly increasing with the lattice distance R . Data are fitted by linear functions. For gluonic/fermionic configurations only data with $R \geq 6/2$ are fitted.

all cases we clearly observe that the presence of fermions reduces the string tension: The backreaction is observed in the full $SU(2)$ theory and also reproduced by the center vortices.

Concerning the geometric structure of the vortex surface we observe that the presence of fermions increases the number of isolated short range fluctuations, see Table 1: without fermions about 6.98% of the P-plaquettes are part of isolated unit cubes, whereas with fermions this proportion increases to 12.45%. The proportion of P-plaquettes belonging to bottlenecks is in total decreased from 27.81% to 24%. Fermions increase the amount of unit cubes, but decrease the amount of bottlenecks.

Restricting the analysis to the long-ranged cluster we observe a decrease of fluctuations, especially bottlenecks, when fermions are present, see Table 2: the proportion of P-plaquettes belonging to bottlenecks is reduced from 28.12% to 24.45%. All other fluctuations are only reduced by about 1%.

From this we can conclude that the presence of fermions causes short range fluctuations to detach from the vortex surface, resulting in a more smooth vortex surface that is surrounded by an increased number of isolated short range fluctuations.

4 Acknowledgement

We thank to Aleksandr Nikolaev, Nikita Astrakhantsev and Andrey Kotov for their cooperation in the early stage of this investigation and to Vitaly Bornyakov for important advice.

References

- [1] G. Savvidy, “Infrared Instability of the Vacuum State of Gauge Theories and Asymptotic Freedom,” *Phys.Lett.* **B71** (1977) 133.
- [2] J. Greensite, *An Introduction to the Confinement Problem*, vol. 821 of *Lect. Notes Phys.* Springer, Berlin, Heidelberg, 2011.
- [3] M. Faber and R. Höllwieser, “Chiral symmetry breaking on the lattice,” *Prog. Part. Nucl. Phys.* **97** (2017) 312–355, [1908.09740](#).

- [4] G. 't Hooft, “On the phase transition towards permanent quark confinement,” *Nuclear Physics B* **138** (1978), no. 1, 1 – 25.
- [5] J. M. Cornwall, “Quark confinement and vortices in massive gauge-invariant qcd,” *Nuclear Physics B* **157** (1979), no. 3, 392 – 412.
- [6] L. Del Debbio, M. Faber, J. Giedt, J. Greensite, and S. Olejnik, “Detection of center vortices in the lattice Yang-Mills vacuum,” *Phys. Rev.* **D58** (1998) 094501, [hep-lat/9801027](#).
- [7] N. Y. Astrakhantsev, V. G. Bornyakov, V. V. Braguta, E. M. Ilgenfritz, A. Y. Kotov, A. A. Nikolaev, and A. Rothkopf, “Lattice study of static quark-antiquark interactions in dense quark matter,” *Journal of High Energy Physics* **2019** (May, 2019) 171, [1808.06466](#).
- [8] P. Weisz, “Continuum limit improved lattice action for pure yang-mills theory (i),” *Nuclear Physics B* **212** (1983), no. 1, 1 – 17.
- [9] G. Curci, P. Menotti, and G. Paffuti, “Symanzik’s improved lagrangian for lattice gauge theory,” *Physics Letters B* **130** (Oct, 1983) 205–208.
- [10] L. Del Debbio, M. Faber, J. Greensite, and S. Olejnik, “Center dominance, center vortices, and confinement,” in *NATO Advanced Research Workshop on Theoretical Physics: New Developments in Quantum Field Theory*, pp. 47–64. 6, 1997. [hep-lat/9708023](#).
- [11] V. Bornyakov, D. Komarov, and M. Polikarpov, “P-vortices and drama of gribov copies,” *Physics Letters B* **497** (Jan, 2001) 151–158.
- [12] R. Golubich and M. Faber, “The Road to Solving the Gribov Problem of the Center Vortex Model in Quantum Chromodynamics,” *Acta Physica Polonica B Proceedings Supplement* **13** (2020) 59–65.
- [13] R. Golubich and M. Faber, “Center regions as a solution to the gribov problem of the center vortex model,” *Acta Physica Polonica B Proceedings Supplement* **14** (2021), no. 1, 87.
- [14] R. Golubich and M. Faber, “Improving center vortex detection by usage of center regions as guidance for the direct maximal center gauge,” *Particles* (2019).
- [15] R. Bertle, M. Faber, J. Greensite, and S. Olejnik, “The structure of projected center vortices in lattice gauge theory,” *Journal of High Energy Physics* **1999** (Mar, 1999) 019–019.
- [16] R. Bertle, “The vortex model in lattice quantum chromo dynamics,” Sept., 2005. doctoral thesis.